Modeling the Hg-Ar low-pressure-discharge positive column: A comparative study

G. Zissis, P. Bénétruy, and I. Bernat
Université Paul Sabatier, 118 route de Narbonne, 31062 Toulouse CEDEX, France
(Received 3 June 1991)

For the description of the low-pressure Hg-Ar positive column a self-consistent collisional-radiative model has been used. Calculations of the population densities for the fundamental and the first five excited Hg levels, electron and rare-gas temperature, and densities have been carried out. All these quantities, except electron temperature, have been evaluated as functions of the radial position in the axially uniform positive column; no assumptions on the radial profiles have been made. Macroscopic quantities such as electric-field strength and radiative power output have been also calculated. A diffusion-controlled positive column has been assumed. The most important collisional processes in the plasma have been taken into account (elastic collisions, electron-atom and atom-atom inelastic collisions including excitation, direct and stepwise ionizations, and also superlastic collisions). Argon excitation and stepwise ionization have been included. Radiation trapping has been taken into account, including pressure broadening of resonance lines due to Ar. In our calculations a non-Maxwellian electron-energy distribution function has been used. Diffusion of the charged particles in the presence of Hg^+ and Ar^+ has been considered. Diffusion of the metastable Hg levels has been taken into account. The results obtained in this paper have been compared to corresponding values given in the literature and detailed discussion of the validity of several models has been carried out.

PACS number(s): 52.25.−b, 52.80.Mg, 51.50.+v

I. INTRODUCTION

The aim of modeling of Hg–rare-gas low-pressure-discharge lamps, which is a necessary complement to experimental investigations, is to predict the optimal operating conditions of these devices. Optimal operating conditions, in the case of certain applications, mean high luminous intensities at selected wavelengths and high efficacy for a large range of ambient temperatures. These operating conditions depend closely on several external parameters such as tube diameter and shape, discharge current, and partial pressures of mercury and rare gas in the positive column plasma.

In practice, it was found to be possible to obtain higher uv-radiation intensities by decreasing the tube diameter. In this case, an important decrease of the discharge current was imposed in order to maintain in the positive column the electron temperature as high as needed to maintain an important selective excitation of the resonant $Hg(6\,^3P_1)$ level without an important increase of the visible radiation lines.

In the literature, numerous experimental and theoretical studies have been devoted to both classical fluorescent lamps ($d=24$–36 mm) and compact fluorescent tubes ($d=8$–12 mm) [1–10]. However, to the authors' knowledge, in the case of extremely narrow diameters (a few mm), there are neither sufficient experimental results nor calculations presently available to draw general conclusions [11]. In this paper we deal with a comparative study of several existing models applied to the fluorescent lamps. A collisional-radiative model with a large range of application, developed by the authors, is used as a discussion basis. A review of the most important models will be presented in Sec. II of this paper, whereas Sec. III will be devoted to the presentation of the theoretical bases of our model. Transport phenomena in the discharge plasma and corresponding atomic data used in this study will be given in Sec. IV. Finally, Sec. V will be devoted to a detailed analysis of our calculation results in a large range of Hg-Ar discharges covering classical fluorescent lamps and as well as extremely narrow discharges. A comparison between our calculations and theoretical and/or experimental results will be given when available.

II. REVIEW OF THE EXISTING MODELS

The theoretical analysis of Hg–rare-gas discharges is sufficiently complex to necessitate the use of simplifying assumptions. In fact, these assumptions restrict seriously the field of application of the models. Thus a concept common to the existing models was that calculations should be in good agreement with experimental data within a more or less restricted range of applications. Under this condition the use of arbitrary adjustable parameters has been justified up to now.

Waymouth and Bitter [5] were able to calculate to a remarkably fair degree of approximation the characteristics of classical Hg-Ar lamps ($d=36$ mm, $I=400$ mA, $p_{Ar}=3$ Torr) by using a simplified atomic transition scheme limited to a few atomic levels. In addition, the use of Ar was limited only to a buffer-gas controlling electron mobility. The latter assumption causes some important divergences between calculations and measurements in the case of low partial pressure of mercury in the positive column, because the excitation and ionization of the argon have been neglected. We take note, on the one hand, of the significant deviation between the

values of the electron mobility used in this work and the experimental values found in the literature [2]. On the other hand, Waymouth and Bitter were forced to increase the resonance radiation trapping by a factor of about 3.5, which contradicts the results of more detailed studies on the resonance radiation trapping [12]. However, the principal purpose of this model was to obtain the simplest possible discharge description to fit the experimental data quantitatively. The great simplicity of use renders this model a powerful tool in describing the physical bases of the discharge and also to obtain valid estimations of the orders of magnitude in several cases of Hg–rare-gas discharge.

Lama *et al.* have also elaborated an analytical model without recourse to numerical techniques [9]. This model was based essentially on the same approximations as those used by Waymouth and Bitter and gives a good approximation of the parametric dependence on the discharge variables. However, the model of Waymouth and Bitter remains more accurate.

Another important limit of these works was to deal with average quantities over the discharge cross section and not to consider the variation of all species with radial position. This restriction did not exist in the earlier work of Cayless [4]. However, the model of Cayless was limited to intermediate partial pressures of mercury because, on the one hand, of the simplified treatment of the resonance radiation trapping in the plasma based on the diffusion of radiation, and, on the other hand, because of the argon treatment as buffer gas only.

Both Cayless and Waymouth adopted a Maxwell-Boltzmann electron-energy distribution function in their calculations. This choice is justified partially by the experimental studies of Kenty [1] and Easley [13]. It is of note that the cross sections used in these studies have been evaluated essentially by Kenty under the hypothesis of a Maxwell-Boltzmann electron-energy distribution function. In low-pressure Hg–rare-gas discharges the local thermodynamic equilibrium conditions are not verified ($T_g \ll T_e$) and more specific calculations of the electron-energy distribution function show that the high-energy region of the electron-energy distribution function may deviate significantly from the Maxwell-Boltzmann shape.

More recently, in the work of Winkler, Wilhelm, and Winkler [8], a collisional-radiative model including several Hg levels ($6\,^1S_0$, $6\,^3P_0$, $6\,^3P_1$, $6\,^3P_2$, $6\,^1P_1$, $7\,^3S_1$, $6\,^3D$) and Hg^+ was coupled with the numerical solution of Boltzmann equation. In this model argon excitation and ionization were also included, but the authors do not take into account the contribution of Ar^+ to the charged-particle diffusion. The resonance radiation trapping treatment was carried out according to Holstein's classical theory [14]. This model is also limited to classical cases because of the average treatment of the positive column under the hypothesis of standard radial profiles of excited and charged species over the tube cross section.

Dakin has established a more complete model in order to calculate the radial behavior of the discharge [10]. The field of validity of this model includes classical and compact fluorescent tubes. In a more recent version of the model a satisfactory treatment of the resonance radiation trapping was included. Inelastic collisions between heavy particles (Hg atoms) were taken into account. However, argon excitation and ionization were neglected and the electron-energy distribution function calculation was based on the simplified two-electron group model of Vriens [15].

III. MODEL DESCRIPTION

A. Basic assumptions

The model developed in this work is based on the following basic assumptions: A uniform steady-state positive column established in a circular-cross-section tube is considered. The discharge is supposed to operate with neither stationary nor running striations, and without oscillations. Under these conditions, the positive column is supposed to be axisymmetric (electrode regions are not actually taken into account); this makes the problem one dimensional along the radius. Axial cataphoresis is avoided by considering a very-low-frequency commutative dc power supply instead of a pure dc source.

The discharge tube contains a constant amount of argon and some mercury vapor. The mercury partial pressure is assumed to be the saturated vapor pressure at the tube cold-spot temperature. The total pressure is assumed to be constant along the radius.

Both mercury and argon may be (de)excited by collisions. In this model we take into account the fundamental $Hg(6\,^1S_0)$ level, the first five $Hg(6\,^3P_0, 6\,^3P_1, 6\,^3P_2, 6\,^1P_1, 7\,^3S_1)$ excited states. We also include the fundamental state of Ar and a virtual excited state Ar^* at 11.65 eV which regroups the $1s_2$, $1s_4$, $1s_3$, and $1s_5$ Ar excited states.

Resonance uv lines, corresponding to radiative decay of mercury at 253.7 and 184.9 nm and argon at 104.8 nm, are considered to be partially trapped in the discharge. Visible radiation is due only to Hg (546.1, 435.8, and 404.6 nm). According to the experimental studies, the visible radiation lines [especially that of Hg at 546.1 nm corresponding to the transition $Hg(7\,^3S_1) \rightarrow Hg(6\,^3P_2)$] can also be partially absorbed in the discharge plasma.

Direct and stepwise ionization from the mercury are considered; direct ionization was very often neglected in previous papers. In this work argon stepwise ionization is also taken into account. Ionization does not occur exclusively by electron impact; collisions between excited mercury atoms at $6\,^3P$ levels may be at least as important for the ion formation in some cases. In fact, calculation results given by Vriens, Keijser, and Ligthart have indicated that associative ionization may even be dominant in the positive column of Hg-Ar low-pressure discharge, particularly at the higher Hg densities [16].

Vriens, Keijser, and Ligthart have considered about eight different ionization processes by means of atom-atom collisions. The most important seem to be

(a) $Hg(6\,^3P_2) + Hg(6\,^3P_2) \rightarrow Hg(6\,^1S_0) + Hg^+ + e^-$,

(b) $Hg(6\,^3P_0) + Hg(6\,^3P_1) \rightarrow Hg_2^+ + e^-$.

In the present paper we take into account process (a) but we neglect process (b) because of the dissociative recombination of the molecular Hg_2^+ ion. This process may ensure an extra loss of electrons and ions sufficient to balance the increase of ion production due to reaction (b).

The maintenance of electrical conductivity in the discharge plasma requires production of electron-ion pairs as fast as they are lost by recombination. In these discharges, a diffusion-controlled positive column is assumed (Schottky's regime). The principal loss process is the diffusion of the electron-ion pairs on the tube wall and recombination at this point, rather than volume recombination. The presence of two ionic species (Hg^+ and Ar^+) in the positive column has an important influence on the charged-particle diffusion process. In this work this phenomenon is taken into account by introducing the concept of the multipolar diffusion as described by Delcroix [17].

The wall sheath is assumed to be, in this approach, infinitely thin and thus can be neglected. In a first approximation this assumption is valid, but when the diffusion characteristic length becomes comparable to the tube radius this hypothesis may introduce a systematic error in the calculations.

Electron temperature is also fixed by the balance between production and loss of the electron-ion pairs. This temperature is considered to be constant along the discharge cross section. This hypothesis is partially justified by using the experimental measurements of Verweij in the case of classical fluorescent tubes [2].

The knowledge of the electron-energy distribution function is imposed on a self-consistent discharge model. The most coherent way of introducing electron-energy distribution function is to solve directly the Boltzmann equation. This is an exhaustive solution because of the relative complexity of the treatment. Thus Vriens has proposed the "two-electron-group" model in order to provide a simple and powerful method to account for deviations from the Maxwellian shape [15]. This model is easy to use but it is physically meaningless, especially in the first-excitation-threshold energy region where a slope discontinuity appears. In this paper we use an analytical approximate solution of the Boltzmann equation for the Hg–rare-gas low-pressure mixtures proposed by Lagushenko and Maya [18]. This approximation takes into account the most important collisional processes and presents the advantage of being analytical, thus computer time decreases considerably. In this study we consider that the electron-energy distribution function is constant over the tube cross section. This assumption may introduce systematic errors when the electron-energy distribution function is deformed because of the "reflection" of electrons on the wall sheath.

B. Governing equations

In order to write the continuity equations of all species we take into account all possible collisional and radiative transitions between the atomic levels. For example, in Fig. 1, the lines show the transitions (collisional or radiative) between the Hg atomic states, which are taken into account in our investigation. Because of the steady-state condition, the production and the decay of each excited level must be equal; we obtain then a balance equation as follows (in the case of species j with number density n_j):

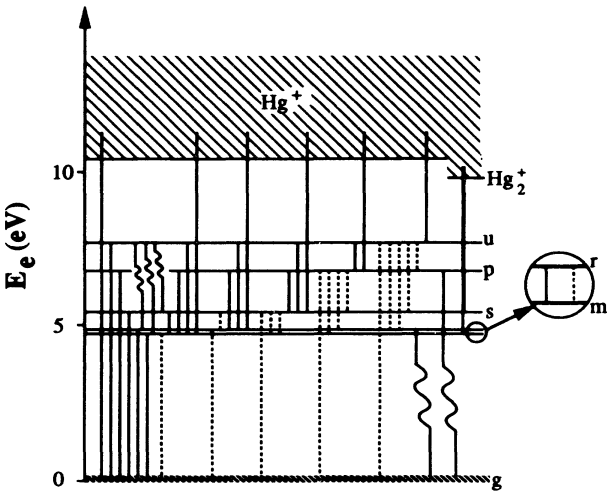

FIG. 1. Simplified atomic structure of Hg used in this paper (g, $6\,^1S_0$; m, $6\,^3P_0$; r, $6\,^3P_1$; s, $6\,^3P_2$; p, $6\,^1P_1$; u, $7\,^3S_1$). Several electron-atom inelastic (solid lines) and second-kind (dashed lines) collisional processes have been included in our calculations, as well as the net radiative transitions (wavy lines) indicated in the figure. An associative ionization process (thick solid line) due to atom-atom collision has been also included.

$$n_e \sum_k (n_k z_{kj} - n_j z_{jk}) + \sum_k (n_k A^*_{kj} - n_j A^*_{jk}) + H_j^{(p)} - n_j H_j^{(d)} + \operatorname{div}\left[D_j N \operatorname{grad}\left[\frac{n_j}{N} \right] \right] = 0 , \quad (1)$$

where $n_e \sum_k n_k z_{kj}$ and $n_e n_j \sum_k z_{jk}$ are the collisional production and decay of the species j by electron impact, respectively; z are the appropriate reaction rate coefficients. The second term includes the gains due to radiative transitions incoming to j level, $\sum_k n_k A^*_{kj}$, and the losses due to radiative (de)excitations outgoing from the same level, $n_j \sum_k A^*_{jk}$; A^* are the total effective transition probabilities for those transitions taking into account the radiation trapping in the plasma. The two terms $H_j^{(p)}$ and $H_j^{(d)}$ correspond to the collisional production and decay of the species j by heavy particle impact; these two terms can be rewritten in a more explicit form as

$$H_j^{(p)} = \sum_l n_l \sum_k n_k Z^l_{kj} , \quad (2a)$$

$$H_j^{(d)} = \sum_l n_l \sum_k Z^l_{jk} . \quad (2b)$$

Z^l_{jk} and Z^l_{kj} are the reaction rate coefficients corresponding to the transitions $j \rightarrow k$ and $k \rightarrow j$, respectively, where particle l is the projectile. The last term of Eq. (1) represents the losses of species j due to the diffusion process to the tube wall (ordinary diffusion for neutral particles and multipolar diffusion for charged particles); D_j is the appropriate diffusion coefficient, N is the total numer-

ic density.

The local energy-conservation equation for the electrons in the positive column can be written in the form

$$Ej_e - P_{\rm el} - P_{\rm in} + P_{\rm sel} - P_{\rm dif} + \mathrm{div}(\lambda_e \,\mathrm{grad} T_e) = 0 \ , \tag{3}$$

where E and j_e are the electric-field strength and electric current density in the positive column; this term represents the energy gain by the electric field. The subscripts el, in, sel, and dif denote elastic, inelastic (excitation and ionization), second-kind collisions, and diffusion contributions, respectively. The last term represents the energy transferred by thermal flux, due to the thermal conductivity of the electron gas; λ_e is the thermal conduction coefficient. In our study, where T_e is taken to be constant, this term is equal to zero. The terms $P_{\rm el}$, $P_{\rm in}$, $P_{\rm sel}$, and $P_{\rm dif}$, can be written in a more explicit form

$$P_{\rm el} = n_e N \sum_j \frac{n_j}{N} \frac{2m_e}{M_j} \langle v_e Q_{ej}^m E_e \rangle \ , \tag{4a}$$

$$P_{\rm in} = n_e \sum_k \left[\sum_{j<k} n_j E_{jk} \langle v_e Q_{jk} \rangle \right] \ , \tag{4b}$$

$$P_{\rm sel} = n_e \sum_k \left[\sum_{j>k} n_k E_{jk} \langle v_e Q_{kj} \rangle \right] \ , \tag{4c}$$

$$P_{\rm dif} = \mathrm{div} \left[D_e^m N \,\mathrm{grad} \left(\frac{n_e}{N} \right) \right] \langle E_e \rangle \ , \tag{4d}$$

where n_e is the electron density; m_e and M_j are the electron mass and the atomic mass of species j, respectively; v_e and E_e are the electron velocity and the electron energy; D_e^m is the multipolar diffusion coefficient of electrons in the presence of Hg^+ and Ar^+; Q_{ej}^m represents the momentum-transfer cross section for the elastic collisions between electrons and atomic species j; Q_{jk} and Q_{kj} are the cross sections for the inelastic and second-kind transitions between the atomic levels j and k, corresponding to an energy gap of E_{jk}. Quantities in brackets, for example, $\langle A \rangle$, represent the mean value of the quantity A: $\langle A \rangle = \int_0^\infty f_e A dv_e$; f_e is the normalized electron-energy distribution function.

The following should be emphasized about Eqs. (4): (i) The elastic collisions between electrons and excited species are negligible because of the very small value of the ratio n_j/N (usually less than 10^{-2}–10^{-3}). (ii) The values $\langle v_e Q_{jk} \rangle$ and $\langle v_e Q_{kj} \rangle$ correspond to the reaction rate coefficients z_{jk} and z_{kj}, respectively. (iii) $P_{\rm dif}$ is usually negligible in the electron-energy balance, but we must not forget that charged species diffusion controls the positive column formation. (iv) The term $P_{\rm in} - P_{\rm sel}$ corresponds to the net radiation loss of the discharge:

$$P_{\rm in} - P_{\rm sel} = P_{\rm rad} = \sum_j n_j \sum_k A_{jk}^* E_{jk} \ . \tag{5}$$

Similarly to Eq. (3), the local energy-conservation equation for the neutral atomic gas can be written as

$$P_{\rm el} - \mathrm{div}(\lambda_g \,\mathrm{grad} T_g) = 0 \ . \tag{6}$$

T_g is the gas temperature and λ_g is the thermal conduction coefficient of the Hg-Ar mixture.

In our case the electric current is imposed by the external circuit; we must then take into account this restriction by including Ohm's law in our equation set (in cylindrical geometry)

$$I = 2\pi \int_0^R r[j_e(r) + j_i(r)] dr = 2\pi E q \int_0^R r \mu_e(r) n_e(r) dr + I_i \ , \tag{7}$$

where q is the elementary charge and μ_e electron mobility. The term I_i accounts for ion contribution to total current, the corresponding ionic current density is j_i; this contribution may be important in the case of a high μ_i/μ_e ratio (μ_i is the ionic mobility).

The numeric densities of the buffer gas ($n_{\rm Ar}$) and of the mercury ($n_{\rm Hg}$) can be evaluated at each radial node by using the ideal gas law

$$n_{\rm Ar}(r) = \frac{p_{\rm Ar}}{k_B T_g(r)} \ , \tag{8a}$$

$$n_{\rm Hg}(r) = \frac{p_{\rm Hg}(T_{\rm cs})}{k_B T_g(r)} \ . \tag{8b}$$

k_B is the Boltzmann constant; $p_{\rm Hg}(T_{\rm cs})$ is the mercury saturated vapor pressure at the tube cold-spot temperature $T_{\rm cs}$; $p_{\rm Ar}$ is the buffer-gas pressure given by the relation

$$\frac{p_{\rm Ar}}{k_B} 2\pi \int_0^R r \frac{1}{T_g(r)} dr = \frac{p_{\rm Ar}(T_f)}{k_B T_f} \pi R^2 \ , \tag{9}$$

where R is the discharge radius and $p_{\rm Ar}(T_f)$ is the initial argon pressure at the tube filling temperature T_f.

Finally, in order to complete our equation set, we use the local charge-neutrality condition in the positive column

$$n_e(r) = n_{\rm Hg^+}(r) + n_{\rm Ar^+}(r) \ . \tag{10}$$

IV. TRANSPORT PHENOMENA AND ATOMIC DATA

The transport phenomena of particles and radiation play a very important role in the positive-column formation. Evaluation of these phenomena depends closely on atomic-data values and often represents a very important calculational task. Another important quantity for the calculation of the particle transport coefficients is the electron-energy distribution function. In this section we will discuss the choice of the atomic data used in this paper and then we will present some comments on the electron-energy distribution function calculation and the particle transport coefficients evaluation. Finally, we will briefly broach the problem of radiation transfer in the plasma.

A. Atomic data

The atomic data used in our investigation include cross-section values for several collisional interactions and natural radiative lifetimes for the excited atomic states.

The electron-Hg momentum transfer and ground-state inelastic cross sections come from Rockwood's paper [19], excitation cross sections of the Hg $6\,^3P_0$, $6\,^3P_1$, $6\,^3P_2$, $6\,^1P_1$, and $7\,^3S_1$ atomic levels are given in the paper by Winkler, Wilhelm, and Winkler [8]. The cross sections for ionization of the excited Hg levels are evaluated by using an analytical expression proposed by Vriens [16]. Figure 2 shows, as an illustration, the electron-Hg ($6\,^1S_0$) inelastic cross sections.

The electron-Ar momentum-transfer cross section is taken from Yousfi and Alkaa's paper [20]. The excitation cross section of the virtual Ar* state is carried out by weighting the excitation cross sections of the four real Ar levels included in the virtual state. These cross sections are given by Gleizes [21]. The ionization cross section for the state Ar* is calculated by using Gryzinski's theory as cited by Drawin [22].

Second-kind-collision cross sections are obtained, in all cases, by using the Klein-Rosseland relation. Concerning the Coulomb interactions between electrons, the cross section comes from Winkler, Wilhelm, and Winkler [8].

It can be noted that in the literature, there are numerous sets of electron-atom (Hg and Ar) collision cross sections which are not always in agreement. The cross sections actually chosen are those which give the best agreement between the measured and calculated electron swarm parameters (drift velocity, ionization coefficient, etc.). Calculation results are carried out by using a Boltzmann computer code presented in the paper of Yousfi *et al.* [23]. Figure 3 shows as an example the electron drift velocities in Ar and Hg in a range of reduced field E/N varying from 10^{-4} to 100 Td. We observe that differences between experiment and calculations remain less than 5% (the present experimental accuracy is 2%) in the total E/N range.

Finally, for the inelastic collisions between Hg($6\,^3P_2$) and Hg($6\,^3P_2$) atoms [reaction (a)], we use an average cross-section value equal to 24×10^{-20} m^2. We estimate this value by adjusting them in order to obtain a satisfactory agreement between our calculations and experimental results in the well-known classical fluorescent tube case at the higher cold-spot temperatures. In fact, some values found in the literature vary from 10^{-20} m^2 (Forester and Franklin [24]) to 100×10^{-20} m^2 (Vriens, Keijser, and Ligthart [16]). Our value is close to that used recently by Sawada, Sakai, and Tagashira [25].

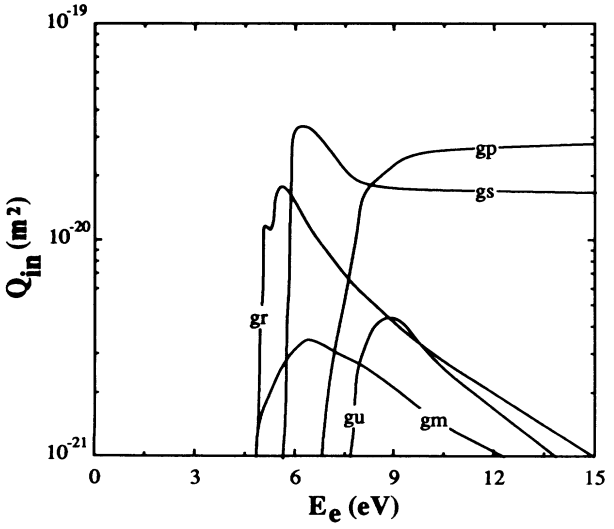

FIG. 2. Inelastic-scattering cross sections for electron-induced direct excitations from the Hg($6\,^1S_0$) level as functions of electron energy.

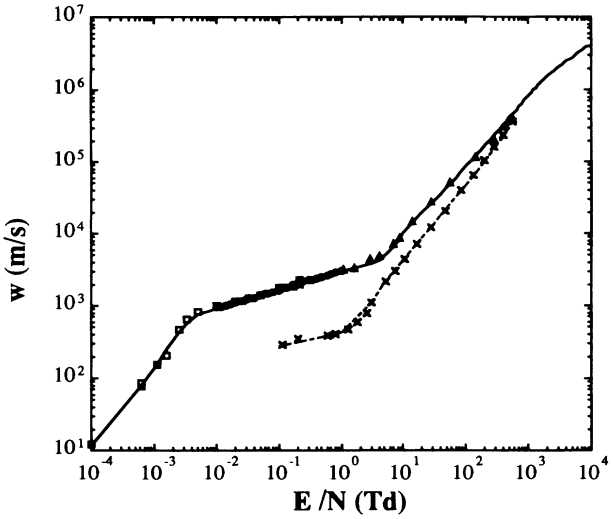

FIG. 3. Comparison between calculated values of the electronic drift velocity in Ar (solid line) and Hg (dashed line) and experimental data (□, Ref. [33]; △, Ref. [34]; ○, Ref. [35]; ×, Ref. [36]).

For the five mercury lines taken into account in this study the natural radiative lifetimes are listed in Table I. The resonant 104.8-nm argon line is also taken into account; its lifetime value is set at 1.96×10^{-9} s.

B. Electron-energy distribution function

As mentioned previously, in this paper we use a non-Maxwell-Boltzmann electron-energy distribution function corresponding to an analytical approximate solution of the Boltzmann equation established by Lagushenko and Maya in the case of Hg–rare-gas low-pressure discharges [18]. Their treatment of the Boltzmann equation accounts for the effects of density gradients and elastic and inelastic collisions between electrons and atoms (Hg and Ar). Elastic collisions between electrons have also been included in this treatment. Yousfi *et al.* [23] have shown that this formula is a good approximation of the Boltzmann equation solution using the two-term method in which all the previously mentioned interactions have been included; in addition, the generation of new electrons by Penning Hg-Ar* ionization and metastable $Hg^{*m}-Hg^{*m}$ interactions are taken into account. Figure 4 shows the different approximations of the electron-energy distribution function in the case of a classical fluorescent tube ($d=36$ mm, $p_{Hg}=7.3$ mTorr, $p_{Ar}=3$ Torr, $I=400$ mA). Damelincourt's experimental data from probe measurements have been also included [6]. Good agreement is observed between experimental

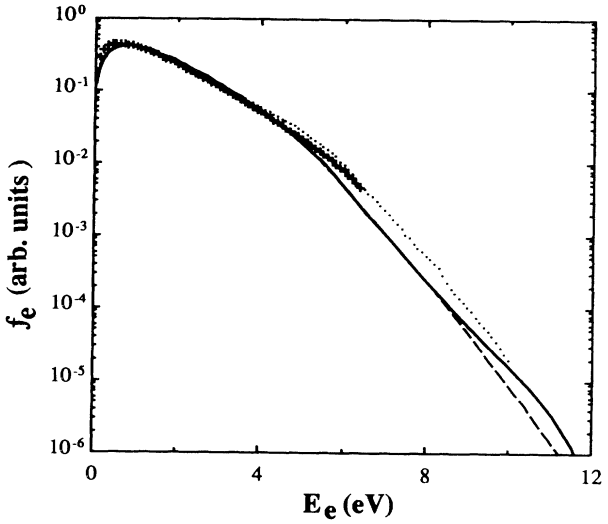

FIG. 4. Electron-energy distribution function in Hg-Ar electric discharge ($p_{Hg}=7.3$ mTorr, $p_{Ar}=3$ Torr, $I=400$ mA, and $d=36$ mm) positive column as function of electron energy. ——, solution of Boltzmann equation; — — —, Ref. [8]; · · · ·, Lagushenko and Maya's analytical formula; +, Damelincourt's experimental data.

data and Lagushenko's formula in the low-electron-energy region (bulk). In the case of the higher electron energies (tail), a satisfactory agreement is also obtained between Lagushenko's calculations and the numeric Boltzmann equation solution. However, this agreement is poorer in the case of low cold-spot temperatures ($T_{cs}<5$ °C); the latter may cause some discrepancies between experimental data and calculations. For this reason we include in the original treatment of Lagushenko and Maya the influence of the electron-Ar inelastic collisions and the interactions between electrons and excited mercury levels.

C. Transport coefficients

Using the isotropic part ϕ_0 of the electron-energy distribution function and the total momentum-transfer cross section Q^m, the electron mobility in the Hg-Ar mixtures may be carried out by using the general formula

$$\mu_e=-\tfrac{1}{3}\left[\frac{2q}{m_e}\right]^{1/2}\frac{1}{N}\int_0^\infty\frac{\sqrt{u}}{Q^m}\frac{\partial\phi_0}{\partial u}du\ , \tag{11}$$

where N is the total numeric density in the positive column. In this study, the Hg-electron elastic collisions are included in our calculations. This term, proportional to $(n_{Hg}/n_{Ar})(Q^m_{eHg}/Q_{eAr})$, constitutes a small correction especially when the mercury density is very low. However, these collisions cannot be neglected especially in high Hg partial pressures where $n_{Hg}/n_{Ar}\approx 10^{-1}$ (because $Q^m_{eHg}/Q^m_{eAr}\approx 10^2$). In this calculation the electron-electron collisions are completely neglected because of the very low ionization degree of the plasma ($n_e/n_{Ar}\approx 10^{-5}$). We note that all other authors have substituted different approximations for relation (11); this may cause large discrepancies between experiment and calculations when we apply these models in some extreme cases.

TABLE I. Wavelengths and natural lifetimes corresponding to radiative transitions of Hg taken into account in this paper.

Transition	Wavelength (nm)	Lifetime (s)
$6\,^3P_2\rightarrow 6\,^1S_0$	253.7	1.08×10^{-7}
$6\,^1P_1\rightarrow 6\,^1S_0$	184.9	1.19×10^{-9}
$7\,^3S_1\rightarrow 6\,^3P_0$	404.6	5.38×10^{-8}
$7\,^3S_1\rightarrow 6\,^3P_1$	435.8	2.36×10^{-8}
$7\,^3S_1\rightarrow 6\,^3P_2$	546.0	1.69×10^{-8}

The value of mercury ion mobility in pure argon is given by Waymouth $\mu_{io}^{Hg^+}(Ar)=1340$ cm^2 V^{-1} s^{-1} Torr (the index o corresponds to standard conditions: 0° C and 1 Torr) [5]. This value is assumed to be almost constant along the positive-column radial position. However, the small minority of mercury atoms has some influence upon the value of the ion mobility because of the charge-exchange process. So, a correction according to Blanc's law is made. The value of $\mu_{io}^{Hg^+}(Hg)$ is equal to 219 cm^2 V^{-1}s^{-1} Torr, as obtained by Hernquist [26]. In the case of very low mercury partial pressures we must take into account the presence of argon ions; the mobility of Ar^+ into Ar is taken to be $\mu_{io}^{Ar^+}(Ar)=1170$ cm^2 V^{-1} s^{-1} Torr.

Taking into account the existence of the two different type of ions (Hg^+ and Ar^+) in the discharge we can evaluate the three multipolar diffusion coefficients (D_e^m, $D^m_{Hg^+}$, and $D^m_{Ar^+}$) as given by Delcroix [17]:

$$bD_e^m=n_{Hg^+}(\mu_i^{Hg^+}D_e-\mu_eD_{Hg^+})+n_{Ar^+}(\mu_i^{Ar^+}D_e-\mu_eD_{Ar^+})\ , \tag{12a}$$

$$bD^m_{Hg^+}=n_e(\mu_i^{Hg^+}D_e-\mu_eD_{Hg^+})+n_{Ar^+}(\mu_i^{Ar^+}D_{Hg^+}-\mu_i^{Hg^+}D_{Ar^+})\ , \tag{12b}$$

$$bD^m_{Ar^+}=n_e(\mu_i^{Ar^+}D_e-\mu_eD_{Ar^+})+n_{Hg^+}(\mu_i^{Hg^+}D_{Ar^+}-\mu_i^{Ar^+}D_{Hg^+})\ , \tag{12c}$$

where $b=n_{Hg^+}\mu_i^{Hg^+}+n_{Ar^+}\mu_i^{Ar^+}-n_e\mu_e$; μ_i are the ionic mobilities at the given conditions of temperature and pressure in the discharge. The binary diffusion coefficients D_e, D_{Hg^+}, and D_{Ar^+} are calculated by injecting the corresponding mobilities in the Einstein's relation. It is easy to verify that if $n_{Ar^+}=0$, we then obtain $D_e^m=D^m_{Hg^+}$ corresponding to the common ambipolar diffusion coefficient D_a.

The binary diffusion coefficient for the fundamental state Hg($6\,^3S_0$) state in the Hg-Ar mixture can be carried out by using the analysis of Hirtchfelder, Courtis, and Bird in the case of a Lennard-Jones interatomic potential [27]. The binary diffusion coefficients for the Hg($6\,^3P_0$) and the Hg($6\,^3P_2$) metastable states are calculated by using a third-degree polynomial adapted to the experimen-

tal data given by Kryukov, Penkin, and Redko [28]. Taking into account that radiative lifetimes are much smaller than diffusion characteristic times, the diffusion of radiative states is neglected.

The thermal conductivity of the Hg-Ar mixture is equal only to the translational thermal conductivity of the binary mixture as given by Hirtchfelder, Courtis, and Bird, and accounts for the presence of the small amount of mercury [27]. The ionization "reaction" components ($Hg+e^- \rightarrow Hg^+ + 2e^-$ and $Ar+e^- \rightarrow Ar^+ + 2e^-$) and the electron-gas contribution have been evaluated and found to be always negligible. If we add, as a test, these terms, the variation of the gas temperature, in the worst case, remains less than 0.1%.

D. Radiation transfer

Resonance radiation trapping is usually treated, in the previous papers, according to Holstein's theory [14]. A preliminary comparison between the effective lifetimes obtained by the latter theory and Monte-Carlo simulations performed in our laboratory has shown that, in the case of extremely narrow tubes, the values obtained by Holstein differ from the Monte Carlo values. In the case of the principal Hg resonance line (253.7 nm) Bernat, Bonneval, and Aubès have performed detailed calculations on the radiation transfer in the discharge Hg-Ar low-pressure plasma as a function of tube diameter and partial pressures of Hg and Ar, respectively [29]. In this work, Doppler effect, natural, and pressure broadening mechanisms have been taken into account. The influence of the fine structure of the line due to the isotopic structure of the natural mercury has been included. The radiation-transfer equation has been solved using the hypothesis of the complete frequency redistribution and a given radial distribution of the excited $Hg(6\,^3P_1)$ state. It has been found that, neglecting all broadening mechanisms other than Doppler effect, the results closely approach Holstein's theory values. However, divergences appear when pressure broadening, due to argon, has been added. These deviations increase with the argon partial pressure. In all cases the average radiation trapping has been found to be less than Holstein's predictions. In the present paper, we take into account the radiation trapping by introducing a constant-along-radius effective transition probability A^*_{254}. This value is found by using Holstein's theory in order to obtain a first approximation A^{*H}_{254} and then we calculate $A^*_{254}=\alpha_{254}(R,p_{Ar})A^{*H}_{254}$ where $\alpha_{254}(R,p_{Ar})$ is a correction factor calculated according to Bernat, Bonneval, and Aubès's work [29]. Figure 5 shows the correction factor α_{254} as a function of the mercury partial pressure for several discharge tube diameters and Ar partial pressures.

The second Hg resonance line (184.9 nm) is also partially trapped in the plasma, but the complete frequency redistribution hypothesis is not valid [12]. We take note that the contribution of the Hg 184.9-nm line remains in all cases less than 15% in the balance equations. Uncertainties due to the collisional cross-section values are greater, thus Holstein's value for radiation trapping may be considered as adequate for our purposes.

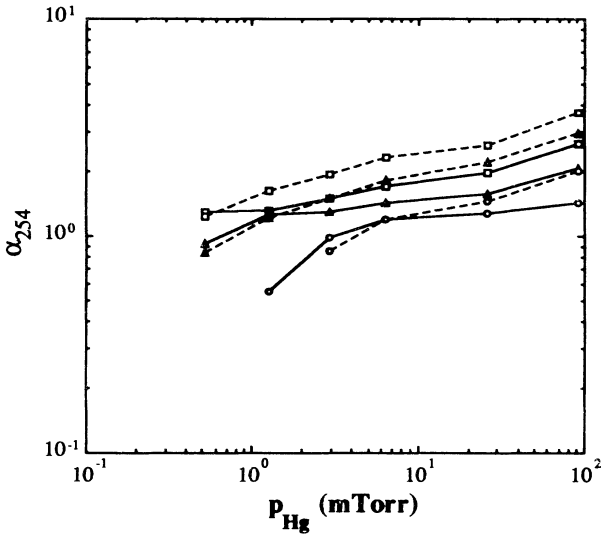

FIG. 5. Correction factor used in the calculation of the effective transition probability of the Hg 253.7-nm resonance line as a function of the Hg partial pressure in the discharge for two Ar filling pressures (——, 3 Torr, — — —, 15 Torr) and several discharge diameters (○, 3 mm; △, 14 mm; □, 36 mm).

The visible mercury lines are also trapped in the discharge plasma, but it is more difficult to take into strict account this trapping. Anyway, the visible radiation represents a small correction in the complete equation set. Hence several authors neglect the visible radiation trapping without great consequences in the calculated values of the main discharge characteristics. However, our calculations without visible radiation trapping has shown that obtained flux of the Hg 546.1-nm line was 40% greater than the experimental values [3]. For this reason, in this paper we include in our calculation an effective escape factor of 60% for the Hg 546.1-nm line; this value is justified by Damelincourt's absorption measurements [6]. In fact, the two other Hg lines (404.6 and 435.7 nm) have been considered less trapped in the plasma (escape factor of about 85%).

V. RESULTS AND DISCUSSION

Calculations are performed in various Hg-Ar discharges. These situations are characterized by the values of several parameters such as tube diameter, discharge current, and partial pressures of Ar and Hg. Table II summarizes these characteristics. In this study, the Hg partial pressure varies from 0.2 to 68 mTorr, corresponding to a cold-spot temperature varying from 0 to 75 °C. The functional relationship between Hg partial pressure and cold-spot temperature used in this paper is given in Ref. [30]. We note that situations denoted by *N* correspond to classical fluorescent tubes with current densities of less than 10^3 A/m^2. Compact fluorescent lamps having current densities in the range of 1.5×10^3 to 3.0×10^3 A/m^2 are characterized by the letter *C*. Finally, some special cases of extremely narrow discharges, noted by *S*, are included in this paper. These discharges have been studied experimentally in our laboratory; their

TABLE II. Main external characteristics (internal tube diameter, Ar partial pressure at 0°C, electric current) of the discharges studied in this work. Family N corresponds to classical fluorescent tubes, C corresponds to compact lamps, and S family represents some special narrow-tube discharges.

Discharge	d (mm)	p_{Ar} (Torr)	I (mA)	j (kA/m^2)
$N1$	36	3	400	0.4
$N2$	36	15	400	0.4
$N3$	24	3	400	0.9
$N4$	24	15	400	0.9
$C1$	14	3	400	2.6
$C2$	14	15	400	2.6
$C3$	14	3	200	1.3
$C4$	10	6	200	2.5
$S1$	6	15	40	1.4
$S2$	6	15	20	0.7
$S3$	3	15	40	5.6
$S4$	3	15	20	2.8

current densities vary widely as shown in Table II.

It is possible to have some indications concerning the field of validity of our model by comparing calculations with the available experimental data in a large range of real situations. For this reason, in the classical $N1$ case we use the experimental data of Verweij [2]. These data are very reliable and are used as references in many studies. Moreover, the measurements of Kreher *et al.* are used for the compact tube $C4$ and the data of Bénétruy for the extremely narrow tube $S2$ [31,32].

Figure 6(a) shows the experimental data and our calculation results for the axial electric-field strength. We note that the experimental accuracy concerning measurements in the $S2$ case has been given ±6%; no information on data accuracy is available for the $N1$ and $C4$ cases. In all cases and for the whole Hg partial pressure range the calculations are in agreement with the experimental data; in fact the observed divergences are still less than ±8% everywhere.

Moreover, Fig. 6(b) gives the calculation results for the emitted radiative power at 253.7 nm. Experimental data corresponding to the three above situations ($N1$, $C4$, and $S2$) are also included in the same plot. Agreement between model and experiment is found to be satisfactory. However, some divergences appear in the case of higher Hg partial pressures ($p_{Hg} > 10$ mTorr); an attempt to explain these systematic deviations will be made later in this section. We take note that the radiation data of Bénétruy was not normalized because of technical problems and thus we multiplied it by a scale factor to bring it into agreement with model. However, on the one hand, in the case $S2$ the position of the maximum Hg 253.7-nm-line emission as a function of Hg partial pressure predicted by the model coincides very well with the experimental results. On the other hand, Bénétruy has carried out some absolute measurements of the maximum 253.7-nm intensities; these values are very close (within ±20%)

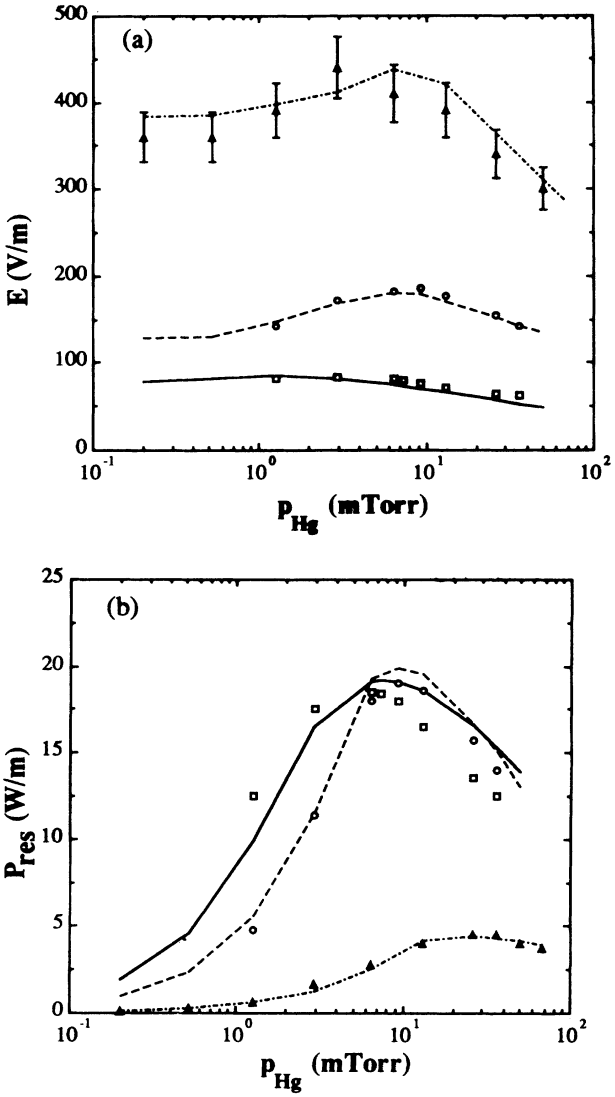

FIG. 6. (a) Comparison between calculated values of the electric-field strength in the positive column and the experimental data for several discharges. Calculations: ——, discharge $N1$; — — —, discharge $C4$; —·—·—·, discharge $S2$. Data: □, Ref. [2]; △, Ref. [31]; ○, Ref. [32]. (b) Comparison between calculated values of the emitted power at 253.7 nm (Hg resonance line) and the experimental data for several discharges. Calculations: ——, discharge $N1$; — — —, discharge $C4$; —·—·—·, discharge $S2$. Data: □, Ref. [2]; △, Ref. [32]; ○, Ref. [31].

to the model predictions. But the experimental accuracy was not satisfactory and thus it is difficult to use these data quantitatively.

Table III summarizes calculated values for electric-field strength, 253.7-nm intensity, electronic temperature, and density as given by several authors for different discharges. Experimental data are also included in this table in order to show the validity of the different models. We note that, on the one hand, in his paper, Dakin unfortunately has only given the total emitted power from the discharge [10]; thus it was not possible to find the intensity of the 253.7-nm resonance line. On the other hand,

the electron temperature given in the same paper was divided into "bulk" and "tail" temperatures; only the bulk values are reported in Table III. For the classical cases, we observe that all models give more or less accurate results; the deviations become more important by increasing the electric current density in the discharge. Thus in the compact case only our calculations and Dakin's model are still accurate. However, we take note that the classical model of Waymouth gives reliable results for these situations, but its field of validity is normally limited to the classical cases. A further increase of the current density challenges the validity of the classical models. However, to the author's knowledge, for the extremely narrow discharges, the only available calculations are carried out by our collisional-radiative model.

Figure 7 shows uv 253.7-nm Hg resonance line-emission intensity as a function of Hg partial pressure. These calculations are repeated for several discharge cases. The dependence of 253.7-nm-line emission on Hg partial pressure can be explained by taking into account the evolution of two competitive factors: excited-state density growth and radiation trapping effect. The radiation trapping process can be significant only when it increases more rapidly than the radiative state density. Since, at low Hg partial pressure (less than 1 mTorr) the relative variation rate of the excited state density is about 3.9 and that of the radiation trapping is 1.1, in higher Hg partial pressure (about 40 mTorr) these rates becomes 0.1 and 0.3 respectively; in this region radiation trapping controls the uv emission. Under these assumptions the presence of a maximum of 253.7-nm emission as a function of the Hg partial pressure is justified. However, the value and the position of this maximum may be different from one situation to another and depend on several discharge parameters as tube radius, Hg and Ar partial pressures, and arc current. In fact, these parameters are related to some more fundamental quantities, such as

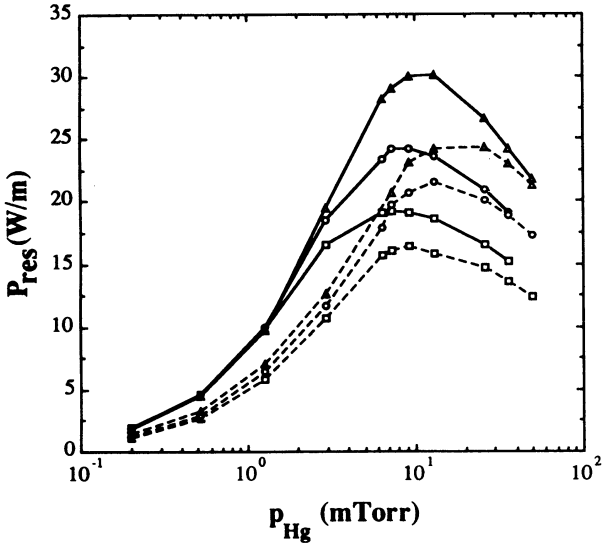

FIG. 7. Emitted power at 253.7 nm (Hg resonance line) as a function of the Hg partial pressure for two different Ar filling pressures (——, 3 Torr; — — —, 15 Torr) and several discharge diameters (□, 36 mm; ○, 24 mm; △, 14 mm).

TABLE III. Comparison between our calculation results and other existing models as well as existing experimental data for various discharge tubes. We compare electric field strength (E), emitted power at 253.7-nm Hg resonance line (P_{res}), axial electronic density [$n_e(0)$], and electronic temperature (T_e). (An asterisk indicates that the model is not valid in this case; a blank indicates data unavailable.)

	Discharge												
	N1	*N3*	*C3*	*C4*	*S2*	*N1*	*N3*	*C4*	*N1*	*N3*	*C3*	*N1*	*N3*	*C3*
T_{cs} (°C)	42	42	43	30	40	42	42	30	42	42	43	42	42	43
P_{Hg} (mTorr)	7.4	7.4	7.9	2.9	6.3	7.4	7.4	2.9	7.4	7.4	7.9	7.4	7.4	7.9
	E (V/m)					P_{res} (W/m)			$n_e(0)$ (10^{17} m^{-3})			T_e (10^3 K)		
Expt.[a]	81	94	154	170	410	18.4	22.2	11.4	5.0	8.0	11.4	11.5	13.0	14.5
This work	80	96	136	169	437	19.1	24.2	11.5	5.1	9.8	9.8	10.9	12.0	14.8
Waymouth[b]	78	96	147	*	*	16.4	19.6	*	5.6	10.6	11.0	10.9	11.8	13.6
Lama *et al.*[c]	92	86	118	170	*	25.7	23.6	18.5	3.8	7.7	11.2	12.2	13.2	14.9
Winkler, Wilhelm, and Winkler[d]	77					19.8			6.8			12.3		
Denneman *et al.*[e]	81	102				20.3	25.0		6.5	12.8		12.4	13.0	
Dakin[f]	80		158						5.5		12.6	13.4		16.3

[a]Reference [10].
[b]References [2,31,32].
[c]Reference [9].
[d]Reference [8].
[e]Reference [7].
[f]Reference [10].

electric current density, elastic-collision number, and radiation trapping.

For given partial pressures, increasing the current density means that electron density increases too. It is known that the electron density is directly related to the collisional process and thus, in a way, more electrons mean more excitation. Accordingly, high electric current density discharges emit more uv radiation. However, the rise of the electron density also causes an important increase of the thermalization degree of the discharge because of the important growth of the elastic-collision process. Thereby the radiative efficiency tends to decrease.

The second important quantity is the elastic-collision process; the electron mobility in the plasma is directly dependent on this process. Increasing the elastic-collision process in the discharge (at constant current density and Hg partial pressure) means that the power dissipated by elastic collisions increases rapidly and thus radiative efficiency decreases. Moreover, the thermalization degree of the plasma rises rapidly by increasing the elastic-collision rate and/or by decreasing radiation escape from the discharge.

The position of the maximum 253.7-nm emission can be explained by using Figs. 8(a) and 8(b). Figure 8(a) shows the dependence of the electron temperature as a function of Hg partial pressure; this behavior will be discussed in the following paragraphs. We observe that electron temperature variation is more rapid in the case of lower Ar partial pressures because of the lower thermalization degree of the plasma. Hence we expect that the functional form of the 253.7-nm emission should be flatter in the case of high Ar filling pressures (e.g., 15 Torr) than in the lower ones (e.g., 3 Torr). Figure 8(b) resumes the dependence of 253.7-nm emission as a function of the electron temperature. By considering the fact that smaller tubes have larger electron current densities and by taking into account the radiation trapping which is proportional to product $p_{Hg}R$ decreases, we conclude that the position of the maximum 253.7-nm emission should be shifted to the higher values of Hg partial pressure by decreasing tube radius.

In Fig. 8(a) we have observed that electron temperature decreases by increasing Hg partial pressure. In fact, the increase of the ionization degree corresponds to a decrease of the electron temperature. In order to explain this observation, a semiquantitative discussion on the equilibrium between the production and loss of charged particles will be given.

The production of electron-ion pair by collisional process is roughly given by the relation $n_e N^* Z_i(T_e)$, where $N^* Z_i(T_e)$ is an "effective" number of ionizing collisions per electron; N^* corresponds to the number density of all the excited species to be ionized (direct ionization is negligible), and Z_i is the total ionization reaction rate. It is known that reaction rates increase rapidly as a function of T_e. For a restricted region of T_e ($5\times10^3 < T_e < 15\times10^3$ K), Damelincourt has considered in a first approximation this functional form to be T_e^n, where the exponent n has a value between 7 and 8 [6]. Hence the average production on the discharge tube cross section is given as $c_1 n_e(0) N^* T_e^n$.

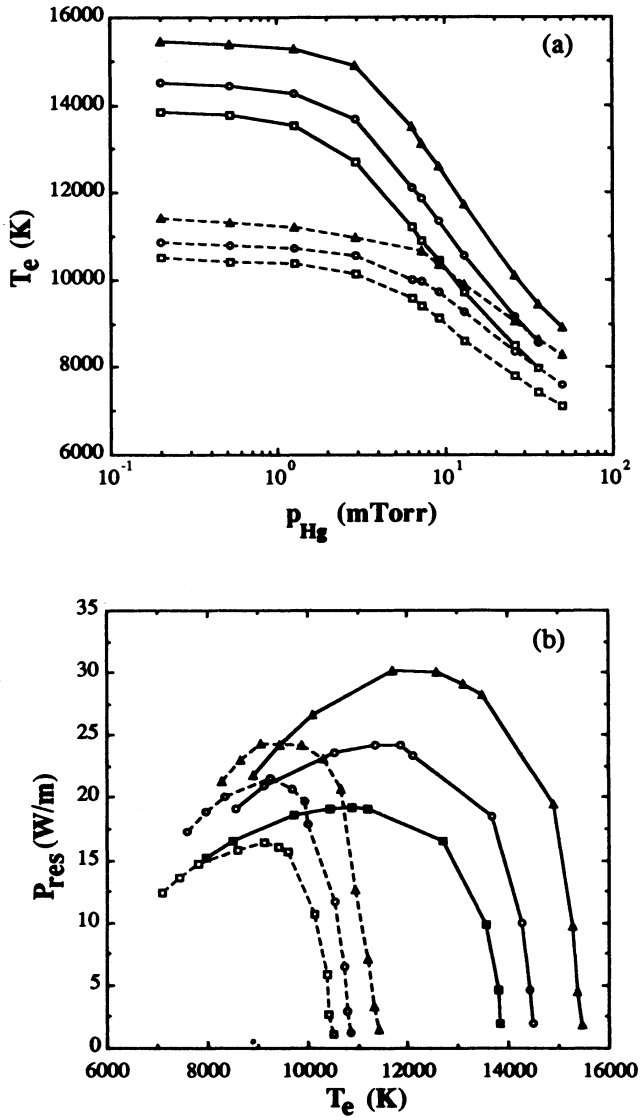

FIG. 8. (a) Electron temperature as function of the Hg partial pressure for two different Ar filling pressures (——, 3 Torr; — — —, 15 Torr) and several discharge diameters (□, 36 mm; ○, 24 mm; △, 14 mm). (b) Emitted power at 253.7 nm (Hg resonance line) as function of the electron temperature in the positive column for two different Ar filling pressures (——, 3 Torr; — — —, 15 Torr) and several discharge diameters (□, 36 mm; ○, 24 mm; △, 14 mm).

The principal electron-ion–pair loss process is the ambipolar diffusion and recombination at the discharge wall. This process is described by the relation $D_a d^2 n_e/dr^2$, but we know that D_a is proportional to $\mu_i T_e$ (in the case where $T_g \ll T_e$), where μ_i is the ion mobility. By averaging this quantity on the tube cross section we obtain a loss process roughly given by $c_2 n_e(0)\mu_i T_e$.

As has previously been said, the production of electron-ion pairs must be equal to the losses; this means that $CN^* T_e^n = \mu_i T_e$. Figure 9 gives a qualitative illustration of these two terms as functions of electron temperature; solid lines correspond to the left-hand term and a

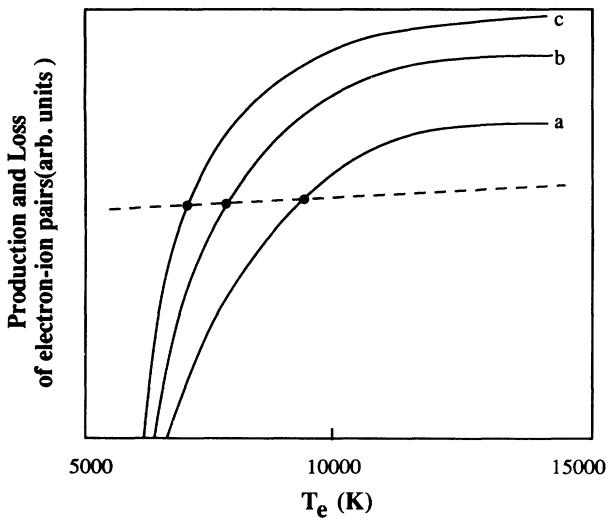

FIG. 9. Qualitative representation of the production (solid lines) and loss (dashed line) terms of the electron continuity equation. Curves *a*, *b*, and *c* correspond to different excited state densities (this quantity increases from curve *a* to curve *c*). The slope of the loss term curve must be equal to ionic mobility in the discharge plasma. Black points corresponding to the intersections of these curves give the electron temperature in the stationary discharge positive column.

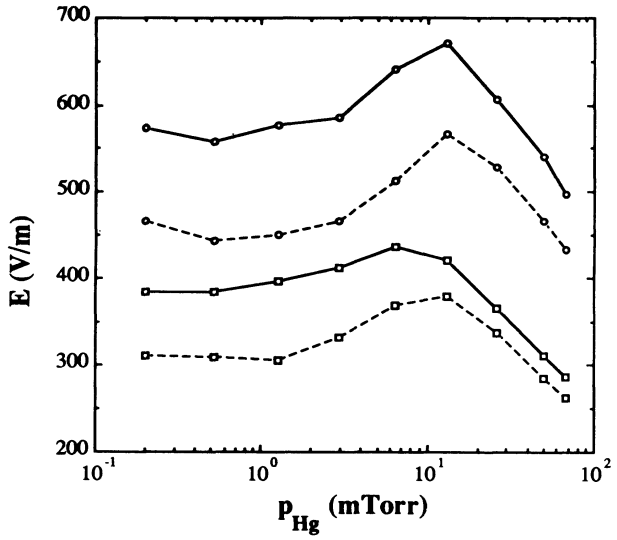

FIG. 10. Electric-field strength in the discharge positive column as function of the Hg partial pressure for two different discharge currents (——, 20 mA; — — —, 40 mA) and two discharge diameters (□, 6 mm; ○, 3 mm) (these values correspond to discharges $S1$–$S4$).

dashed line represents the right-hand term. Only the values of T_e corresponding to the intersection points verify the previous equality; for a given N^* this value of T_e is the electron temperature of the discharge. In Fig. 9 we observe that increasing N^* causes a fall in the electron temperature in order to maintain the equilibrium between the production and loss rates.

Another important parameter for the description of positive-column behavior is axial electric-field strength. For discharges in which electric current is fixed, the axial electric-field strength is directly proportional to the total power losses from the positive column. Figure 10 shows the calculated values of the axial electric-field strength in the four extremely narrow cases ($S1$–$S4$) as functions of Hg partial pressure. The increase of electric current density by decreasing tube radius is responsible for the rise of collisional process in the plasma and thus the total power losses should go up. Hence we can predict the dependence of the electric-field strength on the discharge radius as illustrated in Fig. 10.

By examining the functional form of the electric field as a function of the Hg partial pressure we observe a maximum value corresponding to the region in which uv emission from the plasma becomes maximum too. The existence of this local maximum in the electric-field strength has been verified experimentally in the case of extremely narrow discharges, as well as in classical ones. However, the theoretical explanation is somewhat difficult. In classical models in which Ar ionization has not been included the electric-field strength obtained monotonically decreases in function of the Hg partial pressure. In fact, the additional ionization due to Ar is responsible for this local maximum. Figure 11 gives the electric-field strength for the classical $N1$ case as it has been carried out from our model with and without Ar ionization. Neglecting Ar ionization means that electron temperature should increase rapidly in the case of low Hg pressures because of the low density which limits the ionization. Hence the total power losses increase essentially because of the important increase of the elastic-collision rate. Argon resonance radiation trapping must be great because of its high partial pressure in the discharge plas-

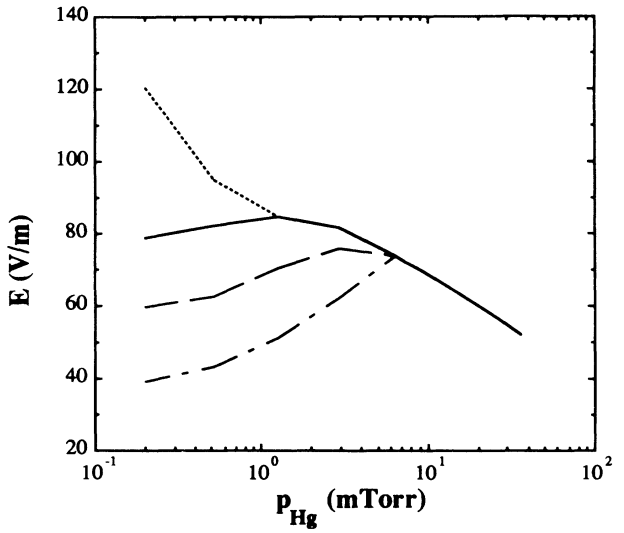

FIG. 11. Calculated electric-field strength in the case of the $N1$ discharge, by taking into account the Ar 104.9-nm resonance line trapping in the plasma. —·—·—·, radiation trapping as given by Holstein theory; — — —, Ar radiation is 10 times more trapped than given by Holstein; ——, Ar radiation is 25 times less trapped than given by Holstein (we keep this value); · · · ·, without Ar emission.

ma. In fact, calculation results for the electric field can be adjusted by choosing an adequate value for effective transition probability of Ar resonance line.

The knowledge of the excited-state densities in the positive-column plasma is very important because the radiation production is directly dependent on these values. In Fig. 12 the axial densities of the three Hg $6\,^3P$ levels in the $N1$ case are presented. Several collisional and radiative processes must be taken into account in order to explain the behavior of the excited-state densities as function of the Hg partial pressure. Electron-induced collisions and radiative transitions are essentially responsible for the production and loss of excited particles. Inelastic collisions between two excited atoms are often neglected in the previous models. In fact, these reactions cannot directly affect particle balances because, on the one hand, their relative weight is about hundred times less than the weight of electron- and photon-induced processes. On the other hand, the relatively low excited-state densities tend to diminish the probability of these reactions. However, collisions between excited Hg* atoms, as the reactions discussed in Sec. III A of this paper, can be considered as additional ionization sources. Hence, as has been said previously, by increasing the ionization degree the electron temperature tends to decrease. On that account, the Hg*-Hg* interactions can indirectly affect the excited-state population. For example, Winkler, Wilhelm, and Winkler, by neglecting the Hg*-Hg* interactions, have found that Hg($6\,^3P$) state densities increase monotonically by increasing Hg partial pressure [8]. However, the experimental data confirms this monotonic increase only for the radiant Hg($6\,^3P_1$) state, the populations of the two metastables Hg($6\,^3P_0$) and Hg($6\,^3P_2$) states "saturate" in the higher Hg partial pressures [3,6].

In this work we have taken into account only one additional ionization reaction between two Hg($6\,^2P_2$) atoms [reaction (a)]. This reaction seems to us to be responsible for the "saturation" of the metastable Hg levels. Moreover, according to its cross-section value, it is possible to fit our calculations to the experimental data. In this way, and for a mean cross section value of 24 Å^2, as shown in Fig. 12 we obtain a satisfactory agreement between data and calculations for the three Hg($6\,^3P$) levels without important perturbations to the obtained values of the axial field strength and Hg 253.7-nm resonance line emission.

For an understanding of the main production and loss procedures of the excited-state atoms, a detailed analysis of their particle balance equations is necessary. Figure 13 shows the most important total collision rates (integrated over the discharge cross section) in dependence on the Hg partial pressure for the three Hg($6\,^3P$) levels. Solid lines correspond to collisional production rates and dashed lines represent the collisional loss rates. In this figure we observe that in the whole Hg partial pressure range, the main production mechanism of metastable Hg($6\,^3P_0$) and Hg($6\,^3P_2$) levels is the direct electron-induced excitation from the ground Hg($6\,^1S_0$) state. The resonant Hg($6\,^3P_1$) level at low and medium Hg partial pressures is essentially produced either by direct excitation from the ground state and from second-kind process from the metastable

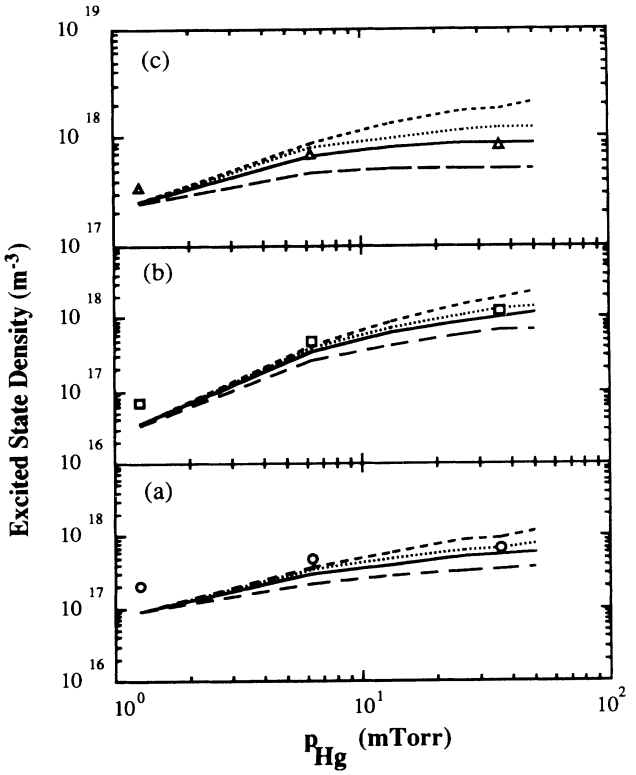

FIG. 12. Axial excited-state densities of the Hg($6\,^3P$) atomic levels (*a*, $6\,^3P_0$; *b*, $6\,^3P_1$; *c*, $6\,^3P_2$) in the case of the $N1$ discharge as functions of the Hg partial pressure. Symbols represent the experimental data given in Ref. 6. The influence of the Hg-Hg inelastic scattering is also illustrated: - - -, without Hg-Hg collisions; ——, with a Hg-Hg inelastic-scattering cross section of 24 Å^2; · · · ·, with a Hg-Hg inelastic-scattering cross section of 10 Å^2; — — —, with a Hg-Hg inelastic-scattering cross section of 100 Å^2.

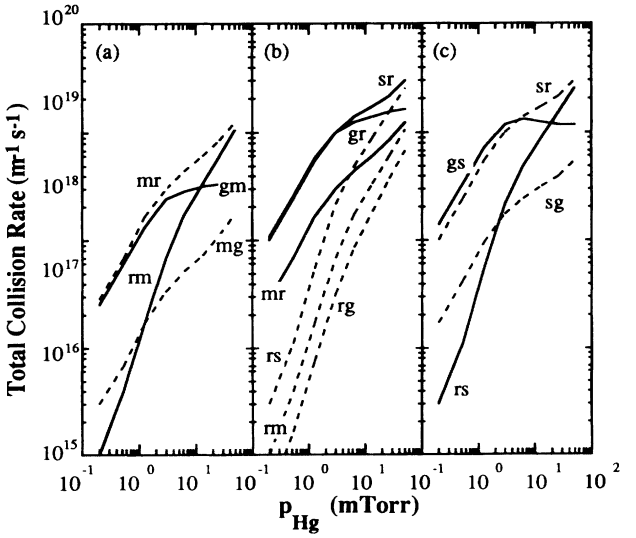

FIG. 13. Total collision rates (integrated on the discharge cross section) for electron induced excitations (solid lines) and 2nd kind collisional (dashed lines) process from/to Hg-$6\,^3P$ excited atomic levels (a) $6\,^3P_0$, (b) $6\,^3P_1$, and (c) $6\,^3P_2$.

$Hg(6\,^3P_2)$ state. However, as Hg partial pressure increases, the relative weight of the reaction $Hg(6\,^3P_2)+e^- \rightarrow Hg(6\,^3P_1)+e^-$ becomes less than that of the direct excitation procedure. This happens because of the rapid growth of all kinds of inverse collisional processes due to the decrease of the electron temperature in the plasma (slow electron number increases in the plasma). For this reason, the collisional losses of the resonant $Hg(6\,^3P_1)$ state is the predominant mechanism at high Hg partial pressures instead of the photon-induced process which dominates the low and medium Hg partial pressure range. Another important remark is that behavior of metastable $Hg(6\,^3P_0)$ and $Hg(6\,^3P_2)$ states changes significantly with the increase of the Hg partial pressure: In low pressures these levels are produced essentially by direct excitation from the ground state and this excitation directly transfers to the radiant state which is deexcited by radiative emission. In higher pressures, radiation trapping increases and on this account the density of the radiant state goes up also; thus a strong coupling between the three $Hg(6\,^3P)$ levels appears and a collisional-like equilibrium seems to be established in this case. The last observation, combined with the fact that electron temperature goes down and neutral particle temperature rises, suggests that the thermalization degree of the plasma increases with the rise of Hg partial pressure. In fact, the mean Boltzmann decrement of the $Hg(6\,^3P)$ levels, as an indication of the thermalization degree of the $N1$ discharge, is found to be 0.08 at 0.2 mTorr and becomes 0.53 at 50-mTorr Hg partial pressure.

Finally, as an application, Fig. 14 gives a rough idea of the distribution of the energy reaching the glass wall in the conditions of maximum production of the 254-nm line; a fraction of this energy should be absorbed at the wall. A comparison between the tube $N3$ and the extremely narrow tube $S4$ shows that, in spite of the fact that in the previous cases volumic power is very different (8.1×10^4 and 1.5×10^6 W/m^3, respectively), energy distribution in the different "channels" is almost similar. We take note that maximum resonance line emission occurs at about 9 and 50 mTorr of Hg partial pressure for the $N3$ and $S4$ tubes, respectively.

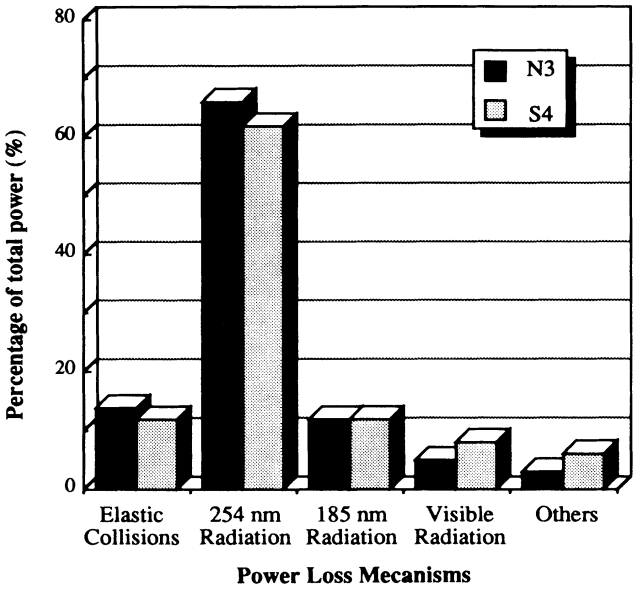

FIG. 14. Energy distribution reaching the tube wall in the conditions of maximum production of the Hg 254-nm resonance line (comparison between $N3$ and $S4$ tubes). Visible radiation is essentially the Hg triplet from the $Hg(7\,^3S_1)$ level. Power losses due to Hg diffusion and Ar resonance radiation are included in "Others."

VI. CONCLUSIONS

In this paper the theoretical bases of a collisional-radiative model have been discussed in detail. This model has been applied to the determination of the radiative and electric characteristics of the Hg-Ar low-pressure discharges. Our calculations have been compared to the available experimental values and to other theoretical calculations. A comparative study of several models applied to the Hg-Ar low-pressure discharges has been carried out in order to define their range of validity.

The results presented in this paper cover a large range of Hg-Ar fluorescent lamps going from classical large tubes ($d=36$ or $d=24$ mm) to narrow special tubes ($d=3$ mm); our calculations have been found in a good agreement with the experiments.

Finally, a detailed discussion on the physical aspects of the Hg-Ar low-pressure discharges has been presented in order to explain our calculation results. However, as was previously noticed, only a modeling of the discharge, including a detailed analysis of the Boltzmann equation, can give more precise information on the Hg-Ar low pressure discharge. This is what we plan to do in the future.

ACKNOWLEDGMENTS

The authors are indebted to Professor J.J. Damelincourt for his useful remarks and directions during this work. We would also like to thank V. Plagnol for his help in the calculations and J.L. Bonneval for his assistance in the realization of this paper. The work reported in this paper was partially supported by CIE Phillips Eclairage (France).

[1] C. Kenty, J. Appl. Phys. **21**, 1309 (1950).
[2] W. Verweij, Philips Res. Rep. Suppl. **2**, 1 (1961).
[3] M. Koedam and A. A. Kruithof, Physica **28**, 80 (1962).
[4] M. A. Cayless, Brit. J. Appl. Phys. **10**, 186 (1959); M. A. Cayless, in *Proceedings of the IV International Conference on Ionization Phenomena in Gases* (North-Holland, Upsala, 1959), Vol. I, pp. 262–277; M. A. Cayless, Brit. J. Appl. Phys. **14**, 863 (1963).
[5] J. F. Waymouth and F. Bitter, J. Appl. Phys. **27**, 122 (1956); J. F. Waymouth, *Electric Discharge Lamps* (MIT Press, Cambridge, 1971).
[6] J. J. Damelincourt, Thèse de doctorat d'Etat, Université Paul Sabatier, Toulouse, 1973.
[7] J. W. Denneman, J. J. de Groot, A. G. Jack, and F.A.S.

Ligthart, J. Illum. Eng. Soc. **10**, 22 (1980).
[8] R. B. Winkler, J. Wilhelm, and R. Winkler, Ann. Phys. (Leipzig) **40**, 89 (1983); **40**, 119 (1983).
[9] W. L. Lama, C. F. Gallo, T. J. Hammond, and P. J. Walsh, Appl. Opt. **21**, 1801 (1982).
[10] J. T. Dakin, J. Appl. Phys. **20**, 563 (1986); L. Bigio and J. T. Dakin, *ibid.* **65**, 375 (1989).
[11] G. Zissis, P. Bénétruy, J. J. Damelincourt, and A. Por, in *Proceeding of the Fifth International Symposium on the Science and Technology of Light Sources,* edited by R. Devonshire (Sheffield University Press, York, 1989), p. 71.
[12] P. van de Weijer and R.M.M. Cremers, *Radiative Processes in Discharge Plasmas* (Plenum, New York, 1986), Vol. B149, p. 65.
[13] M. A. Easley, J. Appl. Phys. **22**, 590 (1962).
[14] T. Holstein, Phys. Rev. **72**, 1212 (1947).
[15] L. Vriens, J. Appl. Phys. **44**, 3980 (1973).
[16] L. Vriens, R.A.J. Keijser, and F.A.S. Ligthart, J. Appl. Phys. **49**, 3807 (1978).
[17] J. L. Delcroix, *Physique des Plasmas* (Dunod, Paris, 1966), Vol. 2.
[18] R. Lagushenko and J. Maya, J. Illum. Eng. Soc. **14**, 306 (1984).
[19] S. D. Rockwood, Phys. Rev. A **8**, 2348 (1973).
[20] M. Yousfi and A. Alkaa, J. Phys. D (to be published).
[21] A. Gleizes, Thèse de doctorat d'Etat, Université Paul Sabatier, Toulouse, 1980.
[22] H. W. Drawin, Commissariat d'Energie Atomique EURATOM Report No. EUR-FC-383, Fontenay, 1967 (unpublished).
[23] M. Yousfi, G. Zissis, A. Alkaa, and J. J. Damelincourt, Phys. Rev. A **42**, 978 (1990).
[24] J. R. Forester and R. N. Franklin, J. Phys. B **2**, 471 (1969).
[25] S. Sawada, Y. Sakai, and H. Tagashira, J. Phys. D **22**, 282 (1989).
[26] K. G. Hernquist, J. Appl. Phys. **27**, 1231 (1956).
[27] J. O. Hirschfelder, C. F. Courtis, and R. B. Bird, *Molecular Theory of Gases and Liquids* (Wiley, New York, 1954).
[28] N. A. Kryukov, N. P. Penkin, and T. P. Redko, Opt. Spektrosk. **42**, 33 (1977) (USSR) [Opt. Spectrosc. **42**, 17 (1977)].
[29] I. Bernat, J. L. Bonneval, and M. Aubès, in *Proceedings of the XXth International Conference on Phenomena in Ionized Gases,* edited by V. Palleschi and M. Vaselli (Institute of Atomique and Molecular Physics, Pisa, 1991), pp. 69 and 70.
[30] A. N. Nesmeyanov, *Vapor Pressure of Chemical Elements* (Elsevier, Amsterdam, 1963).
[31] J. Kreher, D. Förster, W. Maier, and H. Güntel, in *Proceedings of the Fifth International Symposium on the Science and Technology of Light Sources* (Ref. [11]), p. 55.
[32] P. Bénétruy, Thèse de l'Université Paul Sabatier, Toulouse, 1990.
[33] J. Dutton, J. Phys. Chem. Ref. Data **4**, 577 (1975).
[34] H. N. Kücükarpaci, H. T. Saelee, and J. Lucas, J. Phys. D **14**, 9 (1981).
[35] L.G.H. Huxley and R. W. Crompton, *The Diffusion and Drift of Electrons in Gases* (Wiley Interscience, New York, 1974).
[36] C. W. McCutchen, Phys. Rev. **112**, 1848 (1985); Y. Nakamura, and J. Lucas, J. Phys. D **11**, 325 (1978).

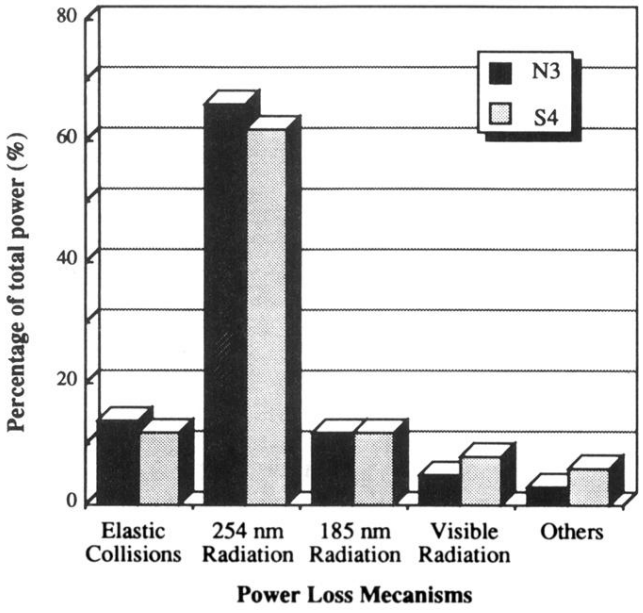

FIG. 14. Energy distribution reaching the tube wall in the conditions of maximum production of the Hg 254-nm resonance line (comparison between $N3$ and $S4$ tubes). Visible radiation is essentially the Hg triplet from the Hg($7\,^3S_1$) level. Power losses due to Hg diffusion and Ar resonance radiation are included in "Others."